

Xuelin ZHANG, Tong ZHANG, Xiaodai XUE, Yang SI, Xuemin ZHANG, Shengwei MEI

A comparative thermodynamic analysis of Kalina and organic Rankine cycles for hot dry rock: a prospect study in the Gonghe Basin

© Higher Education Press 2020

Abstract Hot dry rock is a new type of geothermal resource which has a promising application prospect in China. This paper conducted a comparative research on performance evaluation of two eligible bottoming cycles for a hot dry rock power plant in the Gonghe Basin. Based on the given heat production conditions, a Kalina cycle and three organic Rankine cycles were tested respectively with different ammonia-water mixtures of seven ammonia mass fractions and nine eco-friendly working fluids. The results show that the optimal ammonia mass fraction is 82% for the proposed bottoming Kalina cycle in view of maximum net power output. Thermodynamic analysis suggests that wet fluids should be supercritical while dry fluids should be saturated at the inlet of turbine, respectively. The maximum net power output of the organic Rankine cycle with dry fluids expanding from saturated state is higher than that of the other organic Rankine cycle combinations,

and is far higher than the maximum net power output in all tested Kalina cycle cases. Under the given heat production conditions of hot dry rock resource in the Gonghe Basin, the saturated organic Rankine cycle with the dry fluid butane as working fluid generates the largest amount of net power.

Keywords hot dry rock, Kalina cycle, organic Rankine cycle, thermodynamic analysis

Received Feb. 13, 2020; accepted May 7, 2020; online Oct. 20, 2020

Xuelin ZHANG

State Key Laboratory of Control and Simulation of Power System and Generation Equipments, Department of Electrical Engineering, Tsinghua University, Beijing 100084, China

Tong ZHANG

State Key Laboratory of Control and Simulation of Power System and Generation Equipments, Department of Electrical Engineering, Tsinghua University, Beijing 100084, China; Jingjing Energy Storage Co., Ltd., Changzhou 213200, China

Xiaodai XUE (✉)

State Key Laboratory of Control and Simulation of Power System and Generation Equipments, Department of Electrical Engineering, Tsinghua University, Beijing 100084, China; School of QiDi (TUS) Renewable Energy, Qinghai University, Xining 810016, China; Jingjing Energy Storage Co., Ltd., Changzhou 213200, China
E-mail: xuexiaodai@tsinghua.edu.cn

Yang SI, Xuemin ZHANG, Shengwei MEI

State Key Laboratory of Control and Simulation of Power System and Generation Equipments, Department of Electrical Engineering, Tsinghua University, Beijing 100084, China; School of QiDi (TUS) Renewable Energy, Qinghai University, Xining 810016, China

1 Introduction

Environmental pollution and energy crisis have become global concerned issues. The application of clean alternative energy sources offers an effective solution to these problems. Hot dry rock (HDR) is a type of high-temperature and moist-free rock mass that is buried deep underground [1]. Therefore, it is categorized as a new type of geothermal resource. Geological exploration and heat-extracting tests have been performed at dozens of HDR sites around the world, and in most cases, the measured temperatures of HDR masses are around or much less than 300°C [2,3]. The heat-collecting system of the HDR resource is referred to as an enhanced geothermal system (EGS), which comprises at least one injection well and one production well drilled through into the targeted HDR mass, with artificially widened seepage channels connecting the bottoms of the wells [2,3]. Although pressurized water is the most used heat carrier for heat extraction and transportation in EGS projects [2–6], the traditional steam Rankine cycle is not suitable to deal with such low or moderate temperature thermal sources [7–10]. Therefore, a mode known as “binary power plant” has been widely adopted in the field of HDR thermal utilization [11–13]. Specially, a thermal power generation cycle with a low-boiling-point working fluid serves as bottoming cycle to match with the topping EGS cycle. Two candidate

bottoming cycles, which are Kalina cycle (KC) and organic Rankine cycle (ORC), have been proven eligible and effective in HDR power plants [10–13].

Using ammonia-water mixture as the working fluid, the KC was initially proposed by Kalina [14] at the end of the 20th century. By adjusting either the ammonia mass fraction (AMF) or the working conditions, an optimal match between the KC and the given heat source can be easily obtained [15]. A family of unique KC system (KCS) has been designed to fit in different application scenarios. To deal with low or moderate temperature thermal sources, three KCSs are recommended: KCS-11 for a thermal temperature of about 121°C to 204°C, and KCS-34 and KCS-34 g for those below 121°C [16–20]. In view of that, some studies have been conducted by mixing up the three KCSs; the present paper takes the earliest available introduction by Mlcak [19] and a review paper by Zhang et al. [20] as references. After the feasibility of the KCS-34 was verified in an experimental power plant in 1996 [21], the first commercial KC-type HDR power plant was successful commissioned in 2000 based on a KCS-34, generating a 2 MW power output at a heat supply of about 120°C [22].

Unlike the KC, the ORC can adopt a variety of pure or mixed fluids as working medium. However, when the temperature of the thermal supply ranges from 100°C to 250°C, the ORCs combined with pure fluids tend to be more energy-efficient than those with mixtures [23]. According to the slope (dT/ds) of the saturated vapor line in the T - s diagram, pure working fluids can be classified into three types: wet fluid with positive slope, dry fluid with negative slope, and isentropic fluid whose slope tends to infinity [7,8,24,25]. For dry fluids and some of the isentropic fluids, it is a common practice to expand them directly from the saturated state [8,9,25,26]. But for wet fluids, superheated expansion is recommended to avoid the potential hazard of droplet-forming at the outlet of the turbine [8,25,26]. Moreover, Chen [24] and Saleh et al. [25] argue that for working fluids at low critical point temperatures, making the fluids supercritical before expansion has a certain advantage. Therefore, the configurations of ORCs include three basic system patterns: ORC with vapor expanding from the saturated state (ORC-S), ORC with vapor expanding from the superheated state (ORC-SH), and ORC with vapor expanding from the supercritical state (ORC-SC). In 2007, the industrial ORC-type HDR geothermal power plant was first demonstrated by the Landau Power Plant, which adopts the ORC-S combined with the pure dry fluids isopentane heated by a 160°C geothermal supply [12,27].

While the performance of the topping cycle EGS is closely related to geological engineering technologies, it is crucial to determine how to convert the extracted heat into electricity conveniently and effectively with the bottoming cycle. Therefore, it is necessary to discuss the pattern of cycle structure and operating conditions through a targeted

study and comparison in a specific application scenario. Besides, the optimization of the AMF value for the KC and the type of fluid for the ORC depend a lot on the specific operating temperature and pressure [23].

Previous studies and projects mainly focused on the KCS-34, the KCS-34 g, and the ORC-S. Given the thermal source temperature as 100°C, Rodríguez et al. [13] selected R-29 for the ORC-S and an AMF of 84% for the KCS-34 as comparative combinations respectively, and found that the net power output of the KC is higher than that of the ORC. The same outcome was delivered by Mergner and Weimer [28] through a comparison between KCS-34 with an 80% AMF and ORC-S with R245fa at 120°C. When the temperature of the thermal source rose to 150°C, however, Lin et al. [29] found that the power output of the ORC-S combined with R245fa is significantly higher than that of the KCS-34 with an AMF of 90%. Fiaschi et al. [30] made a comparison between ORC-S with R1233zd(E) and KCS-34 with an AMF of 84.55% and claimed that when the temperature of the thermal source is 120°C, the maximum electrical power generated by the KC is more than that of the ORC; however, raising the temperature to 212°C, it turns out just the opposite. After studying the waste heat recovery of the solid oxide fuel cell/gas turbine exhaust of about 200°C to 250°C, Gholamian and Zare [31] pointed out that the ORC-S combined with R113 provides a significantly higher power output than the KCS-34 with an AMF mixture of 82%. Other works on the KCS-34/KCS-34 g and the ORC-S have presented consistent findings that the KCS-34/KCS-34 g does not have advantages over the ORC-S when it comes to the thermal sources of over 120°C [32–34]. It was also confirmed that the reducing in operation pressure, turbine size and expansion ratio, and heat transfer area have a positive impact on the economic performance of the bottoming cycle [35–37].

However, probably because the application of HDR just begins in recent years in most areas, only a demonstration project and two theoretical researches based on the KCS-11 were made public without comparison with any ORCs [16,38,39]. It is necessary to make a case-by-base study to ascertain how different they would perform under the same given HDR thermal conditions.

In the present paper, the most suitable bottoming cycles for the high-quality HDR resource first identified in the Gonghe Basin, Qinghai province, China is mainly studied. Besides, seven AMFs are separately introduced to a KCS-11 based model, and the three different ORC configurations severally combined with nine working fluids are systematically tested. In addition, the thermodynamic performances, including net power output, energetic efficiency, mass specific power, and volume specific power, are comparatively analyzed. Moreover, in view of the main profit from electricity generated, the maximum net power output is taken as the key evaluation indicator of the cycle performance. Furthermore, exergy efficiency and exergy destruction of the selected bottoming cycles are

also involved. This paper will help decision makers plan the application of local HDR resource in the Gonghe Basin, thus facilitating the further study and application of technologies for the utilization of HDR resource in China.

2 Description of the site studied

The Gonghe Basin is located about 50 km west to the city of Xining and 30 km south to the Qinghai Lake [40]. In August 2017, prospectors detected an HDR mass of 236°C from the GR1 well at a depth of 3705 m [41], releasing the highest-temperature HDR resource found in China so far.

Figure 1 demonstrates the 30 HDR sites around the world [2,3,42–49]. The oblique line denotes the general gradient of formation temperature variation with the increase in depth, which is 0.03°C/m [50]. Noteworthy, the parameters of the GR1 well are very close to those of the Fenton Hill Project [46–49], both of which are significantly above the general gradient line. It is convinced that the GR1 well will obtain a similar heat production by adopting the same EGS technology and heat carrier with the Fenton Hill project, as listed in Table 1. These heat production parameters are used as given conditions for the bottoming cycle analysis in this paper.

3 Description of bottoming cycles

In a binary HDR power plant, the hot water discharged from the production well is first filtered, and then enters the heat-exchangers connected to both the topping and the bottoming cycles to release heat. Finally, it returns to the EGS through the injection well to be heated up again. For the huge quantity of the HDR thermal reservoir, the working conditions of the topping cycle are taken stable as given in Table 1.

The schematic diagrams of three KCSs are illustrated in Fig. 2. According to Refs. [16–20], the KCS-11 as shown in Fig. 2(a) is selected to deal with the given conditions. Figure 3 exhibits the corresponding T - s diagram. After being pumped from the state K1 to the state K2, the ammonia-water mixture is first heated up to the state K3 through the low-temperature (LT) recuperator. Then, the preheated mixture splits into two branches, which are sent to the high-temperature (HT) recuperator and evaporator respectively. The two branches of fluid merge again at the inlet of the superheater (the state K4). To prevent the merger from exergy destruction, the temperatures at the state K4a and the state K4b are set to the same value. Therefore, the process curve of the HT recuperator exactly coincides with that of the evaporator in Fig. 3. The super heater further heats the merged mixture to the superheated state K5 with the heat carrier from the topping EGS. Next,

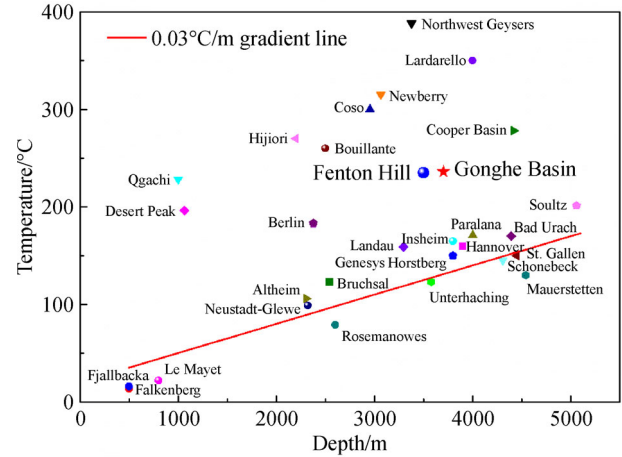


Fig. 1 Parameters of HDR resources surveyed worldwide.

Table 1 Data of the Fenton Hill Project and the GR1 well in the Gonghe Basin

HDR resource	D/m	$T_{HDR}/^{\circ}C$	$m_{pro}/(t \cdot h^{-1})$	$T_{pro}/^{\circ}C$
Fenton Hill	3500	235	> 20	183–190
Gonghe Basin	3705	236	20	185

the overheated vapor expands in the turbine, releasing most of the heat and generating electricity. After recovering the residual heat through the HT and LT recuperators consecutively, the exhaust flow from the turbine is finally cooled down to the initial state K1 by cooling the water in the condenser.

Figures 4 and 5 show the ORC configuration adopted in this paper and the T - s diagrams corresponding to different ways of expansion, respectively. In Fig. 4, the fluid is pumped through the recuperator and the heater successively along the O1-O2-O3-O4 route. The vapor at the state O4 can be saturated, superheated or supercritical, as shown in Figs. 5(a)–5(c), respectively. Then, the vapor expands through the turbine where the thermal energy converts into power. After that, the exhausted low pressure vapor at the state O5 is transported into the recuperator to recycle afterheat, and it is finally cooled down to the state O1 through the condenser. Dry fluids can always keep the expansion process away from their negative saturated vapor lines in the ORC-S, as shown in Fig. 5(a). But most wet fluids with a positive saturated vapor line need to operate in the ORC-SH to prevent them from expanding into the two-phase zone, as shown in Fig. 5(b). Expanding from supercritical state is another effective solution that is worth testing, as shown in Fig. 5(c). The three types of ORC are simulated and compared in this paper using different fluids.

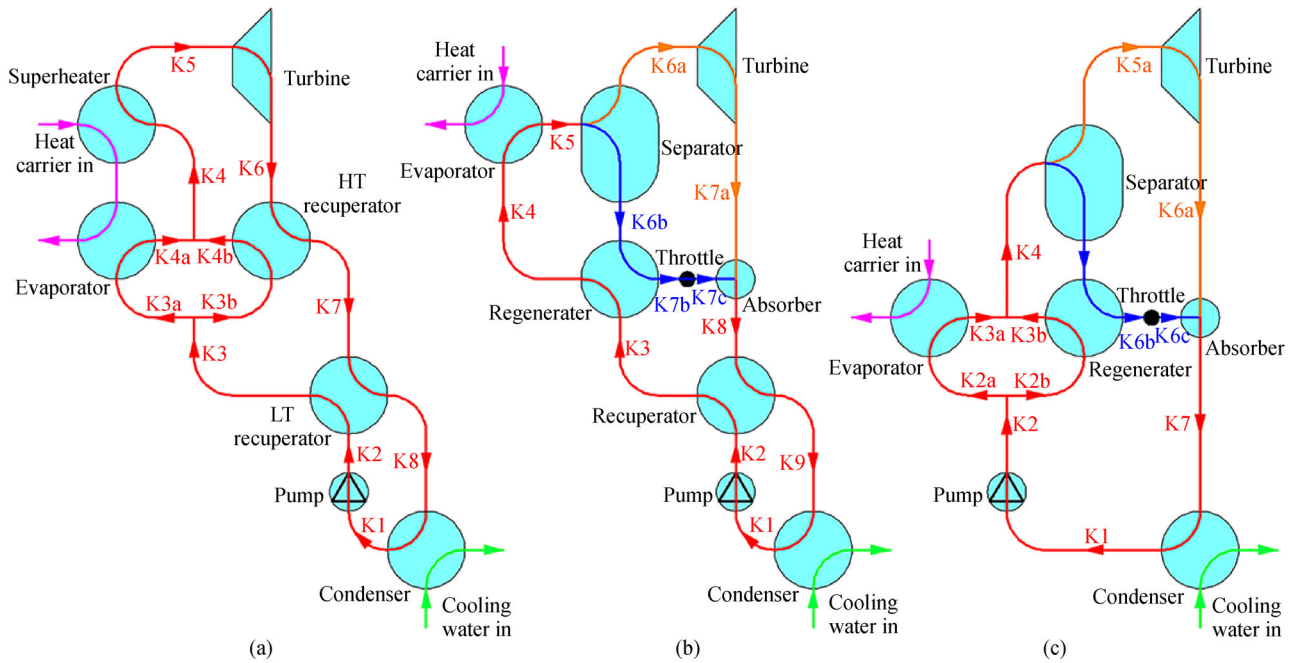


Fig. 2 Schematic diagrams of three KCSs. (a) KCS-11; (b) KCS-34; (c) KCS-34 g.

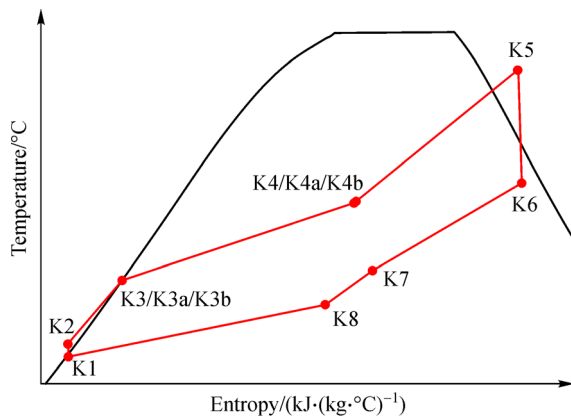


Fig. 3 *T-s* diagram of KCS-11.

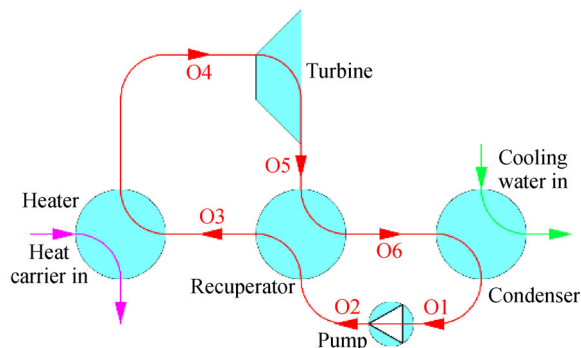


Fig. 4 Schematic diagram of ORC-S, ORC-SH, and ORC-SC.

4 Thermodynamic analysis model

4.1 Assumptions and criteria

In this paper, calculation is conducted using the commercial software package ThermoFlow® Version. 28, and the properties of the working fluids are also drawn from its database. It is assumed that the temperature of the cooling water supply is 30°C, and the maximum temperature rise of cooling water through the condenser is limited to 5°C. Besides, the temperature difference at pinch point is 3°C in the condenser and 5°C in the other heat exchangers [13,26,28,30,51]. For all heat exchangers, the heat leakage rate is 2% and pressure drops is 1% [31,36,51]. In addition, the isentropic efficiencies of the turbines and pumps are chosen as 85% and 75% [13,16,24–26,28,31,32,36,37,39], respectively. Moreover, in view of practical application, the possible maximum operating pressure is restricted under 100 bar. Furthermore, the vapor quality (vapor dryness) at the turbine outlet is kept not lower than 0.9 [24,52].

The net power output W_{net} is used as the main evaluation index to optimize and compare different combinations of bottoming cycle and defined, expressed as

$$W_{net} = W_{turbine} - W_{pump}, \quad (1)$$

where $W_{turbine}$ and W_{pump} are the power output of the turbine and the power consumption of the pump respectively, which are calculated as

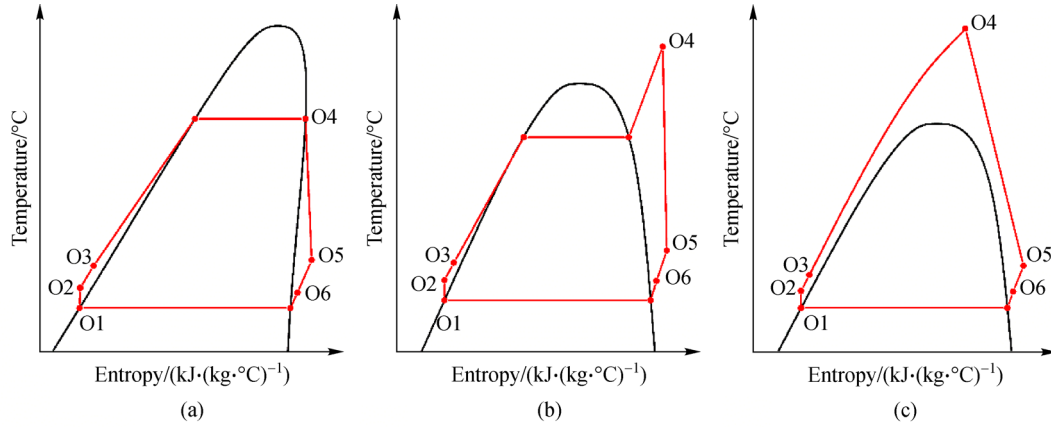


Fig. 5 T - s diagrams.
(a) ORC-S; (b) ORC-SH; (c) ORC-SC.

$$W_{\text{turbine}} = m_{\text{turbine}} \eta_{\text{turbine}} (h_{\text{turbine,in}} - h_{\text{turbine,out}}), \quad (2)$$

$$W_{\text{pump}} = m_{\text{pump}} \frac{(h_{\text{pump,out}} - h_{\text{pump,in}})}{\eta_{\text{pump}}}, \quad (3)$$

where $h_{\text{turbine,in}}$, $h_{\text{turbine,out}}$, $h_{\text{pump,in}}$, and $h_{\text{pump,out}}$ signify the specific enthalpy at the inlets and outlets of the turbine and the pump, respectively; and η_{turbine} and η_{pump} severally represent the isentropic efficiency of the turbine and the pump.

In addition, the thermal efficiency, exergy efficiency, mass specific power, and volume specific power are defined to further investigate the thermodynamic properties of each bottoming cycle.

According to the First Law of Thermodynamics, the thermal efficiency η_{th} is defined as

$$\eta_{\text{th}} = \frac{W_{\text{net}}}{m_{\text{pro}}(h_{\text{pro}} - h_{\text{inj}})}, \quad (4)$$

where m_{pro} refers to the mass flowrate of the heat carrier, and h_{inj} and h_{pro} are the specific enthalpy of the heat carrier at the inlet of the injection well and the outlet of the production well, respectively.

The specific exergy e_i at each state point is calculated as

$$e_i = (h_i - h_0) - T_0(s_i - s_0), \quad (5)$$

where h and s are the specific enthalpy and specific entropy, and the subscripts i and 0 represent the target state point number and the ambient condition, respectively.

Then, according to the second law of thermodynamics, the exergy efficiency η_{ex} of each bottoming cycle can be derived as

$$\eta_{\text{ex}} = \frac{W_{\text{net}}}{m_{\text{pro}}(e_{\text{pro}} - e_{\text{inj}})}, \quad (6)$$

where e_{inj} and e_{pro} represent the specific exergy of the heat

carrier at the inlet of the injection well and the outlet of the production well, respectively.

Further, the mass specific power w_m is defined as the ratio of W_{net} to m_{pump} , which can reflect how much power it can generate with the same quantity of working fluid, and expressed as

$$w_m = \frac{W_{\text{net}}}{m_{\text{pump}}}. \quad (7)$$

The cost of the turbine has a notable influence on the initial investment of the bottoming cycle. The volume flowrate $v_{\text{turbine,in}}$ of the working fluid at the turbine inlet determines the geometric dimensions of the turbine. Therefore, the volumetric specific power w_v is another important index to evaluate the performance of the bottoming cycle, which is defined as

$$w_v = \frac{W_{\text{net}}}{v_{\text{turbine,in}}}. \quad (8)$$

Table 2 lists the exergy destruction and exergy efficiency of each device during a cycle. In Table 2, the heat exchanger includes all types of heat transfer equipment in each cycle, and the subscripts hot and cold signify the exothermic side and endothermic side, respectively.

4.2 Working fluids for bottoming cycles

For the KCS-11, ammonia-water mixtures of seven different AMFs from 76% to 88% with an interval of 2% were selected for simulation and comparison.

The following principles are considered in the selection of the working fluids for the ORCs: According to Ref. [23], common and available pure working fluids are preferred. Besides, in consideration of the low-carbon and environmental protection concept, the working fluids that may destroy the ozone layer and aggravate the greenhouse

Table 2 Exergy destruction and exergy efficiency of each device

Items	Exergy destruction	Exergy efficiency
Pump	$m_{\text{pump}}(e_{\text{pump,in}} - e_{\text{pump,out}}) + W_{\text{pump}}$	$\frac{m_{\text{pump}}e_{\text{pump,out}}}{m_{\text{pump}}e_{\text{pump,in}} + W_{\text{pump}}}$
Turbine	$m_{\text{turbine}}(e_{\text{turbine,in}} - e_{\text{turbine,out}}) - W_{\text{turbine}}$	$\frac{W_{\text{turbine}}}{m_{\text{turbine}}(e_{\text{turbine,in}} - e_{\text{turbine,out}})}$
Heat exchanger	$m_{\text{hot}}(e_{\text{hot,in}} - e_{\text{hot,out}}) - m_{\text{cold}}(e_{\text{cold,out}} - e_{\text{cold,in}})$	$\frac{m_{\text{cold}}(e_{\text{cold,out}} - e_{\text{cold,in}})}{m_{\text{hot}}(e_{\text{hot,in}} - e_{\text{hot,out}})}$

effect (e.g., CFCs, HCFCs, HCFs, and FCs) should not be used in the Gonghe Basin [53]. Moreover, the critical temperature of the chosen fluid should be higher than the temperature of the cooling water supply (30°C). Furthermore, the saturation pressure at ambient temperature is moderately higher than the ambient pressure (1 bar) to avoid vacuum or ultrahigh pressure conditions in the condenser [54].

Based on the above-mentioned principles, nine proper organic fluids are selected and tested selectively with the ORC-S, ORC-SH, and ORC-SC, as listed in Table 3.

5 Results and discussion

With the turbine inlet temperature determined by the pinch point temperature of the superheater, a series of simulations on the KCS-11 and the three ORC configurations were conducted and compared by changing the selected working fluids and the turbine inlet pressure, $P_{\text{turbine,in}}$.

5.1 Analysis of bottoming KCS-11

The bubble point pressure of ammonia-water mixture drops with the AMF decreasing. If the bubble point pressure becomes lower than the tested $P_{\text{turbine,in}}$, the inlet fluid will be a two phase flow.

Figure 6 displays the calculation results of the KCS-11 with different AMFs. To prevent turbine blades from droplet damage, the working pressure range was reduced for an AMF below 82%. According to the W_{net} curves in Fig. 6(a), there are peaks of net power output in the range of 30 bar to 35 bar for most AMFs. The AMF of 82%

allows the KCS-11 to provide a maximum W_{net} at the turbine inlet pressure of 35 bar. Further raising or lowering the AMF both result in a worse W_{net} . The performance of the η_{th} , w_{m} , and w_{v} remains consistent with each other. The indicators are improved with the raising of either the AMF or the $P_{\text{turbine,in}}$, as shown in Figs. 6(b)–6(d). Although the thermal efficiency and specific power can be higher by applying a stronger AMF or a higher $P_{\text{turbine,in}}$, the KCS-11 combined with an AMF of 82% and a $P_{\text{turbine,in}}$ of 35 bar is proposed as the suitable KC combination because generating more electricity brings in higher profits in the long run.

5.2 Analysis of bottoming ORCs

For the wet fluids in Table 3, the ORC-SH and ORC-SC were successively configured by shifting the $P_{\text{turbine,in}}$. Correspondingly, the ORC-S and ORC-SC patterns were both applied to the dry fluids.

The analysis results of ORCs combined with the wet fluids are depicted in Fig. 7 in which the fluid names are arranged in ascending order of T_c from left to right at the top. Because the $P_{\text{turbine,in}}$ varies coherently, the performance points of each fluids in Fig. 8 form continuous curves, where the solid and hollow signs refer to the ORC-SH and the ORC-SC, respectively. In the view of T_c , all the four indicators become better when the ORC-SH combines with a fluid of a higher T_c , but do not show clear regulation when they come to the ORC-SC zone. Figures 7(a)–7(c) suggest that making the vapor at the turbine inlet supercritical is indeed effective within a limited $P_{\text{turbine,in}}$ range to promote the W_{net} , η_{th} , and w_{m} , while it is always good for the w_{v} , as illustrated in Fig. 7(d). Therefore, a

Table 3 Parameters of 9 candidate fluids for the ORCs

No.	Fluids	$T_c/^\circ\text{C}$	P_c/bar	$T_0/^\circ\text{C}$	P_0/bar	Type	
1	Propylene	R-1270	91.06	45.55	−47.91	13.05	wet
2	Propane	R-290	96.74	42.51	−42.42	10.79	wet
3	Cyclopropane	HC-270	125.15	55.60	−31.76	8.27	wet
4	Dimethylether	RE-170	127.15	53.41	−25.11	6.80	wet
5	Propyne	−	129.23	56.26	−25.44	6.71	wet
6	Isobutane	R-600a	134.66	36.29	−12.09	4.05	dry
7	Butane	R-600	151.97	37.96	−0.84	2.83	dry
8	Neopentane	−	160.59	31.96	9.14	2.01	dry
9	Isopentane	R-601a	187.20	33.78	27.45	1.09	dry

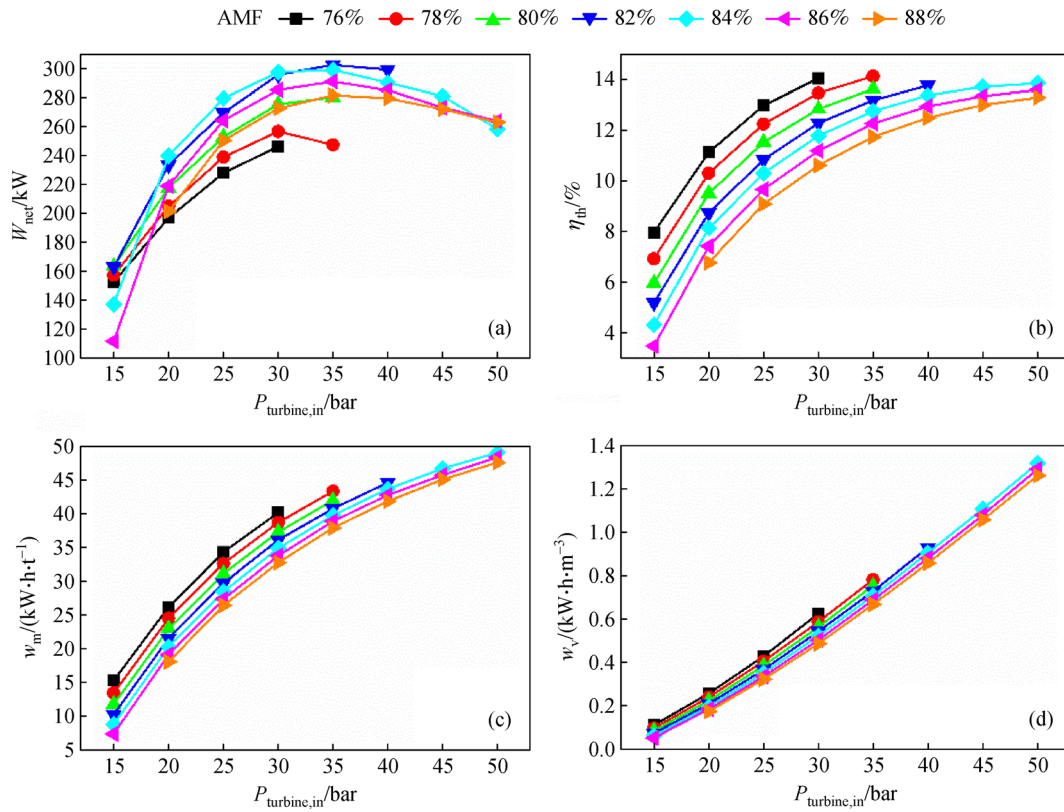


Fig. 6 Performance of KCS-11 with different AMFs.

(a) W_{net} ; (b) η_{th} ; (c) w_m ; (d) w_v .

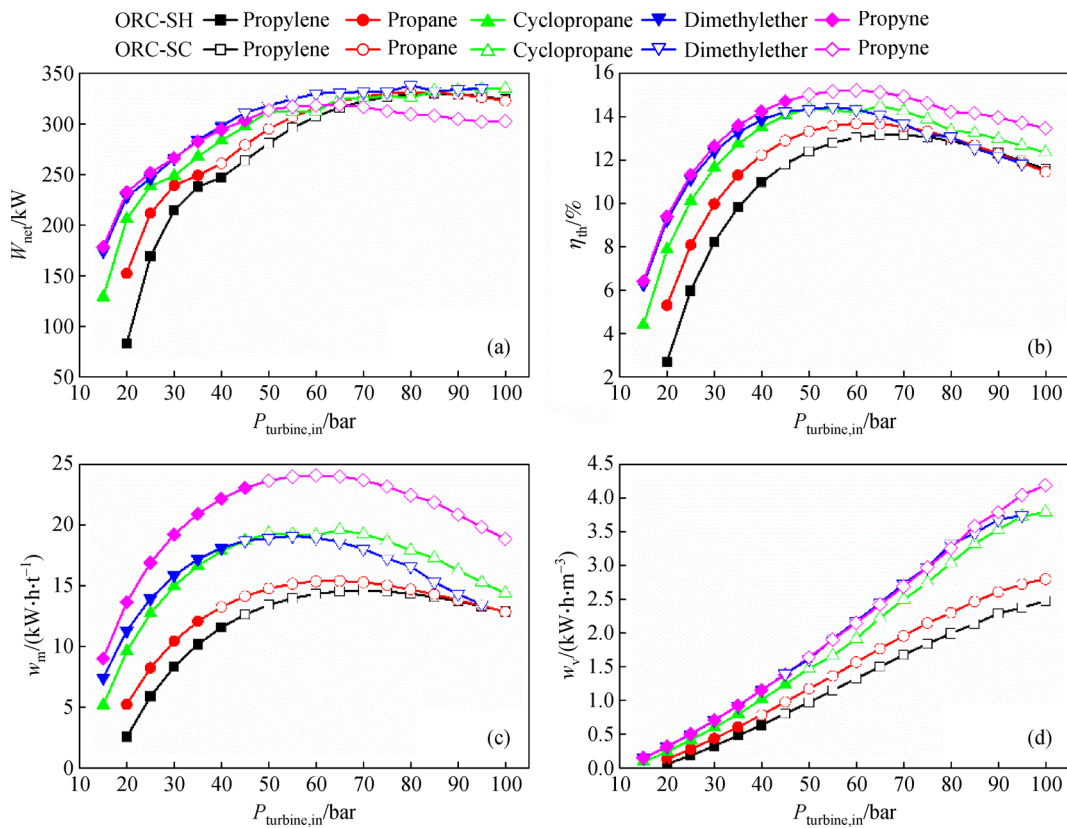


Fig. 7 Performance of ORCs with different wet fluids.

(a) W_{net} ; (b) η_{th} ; (c) w_m ; (d) w_v .

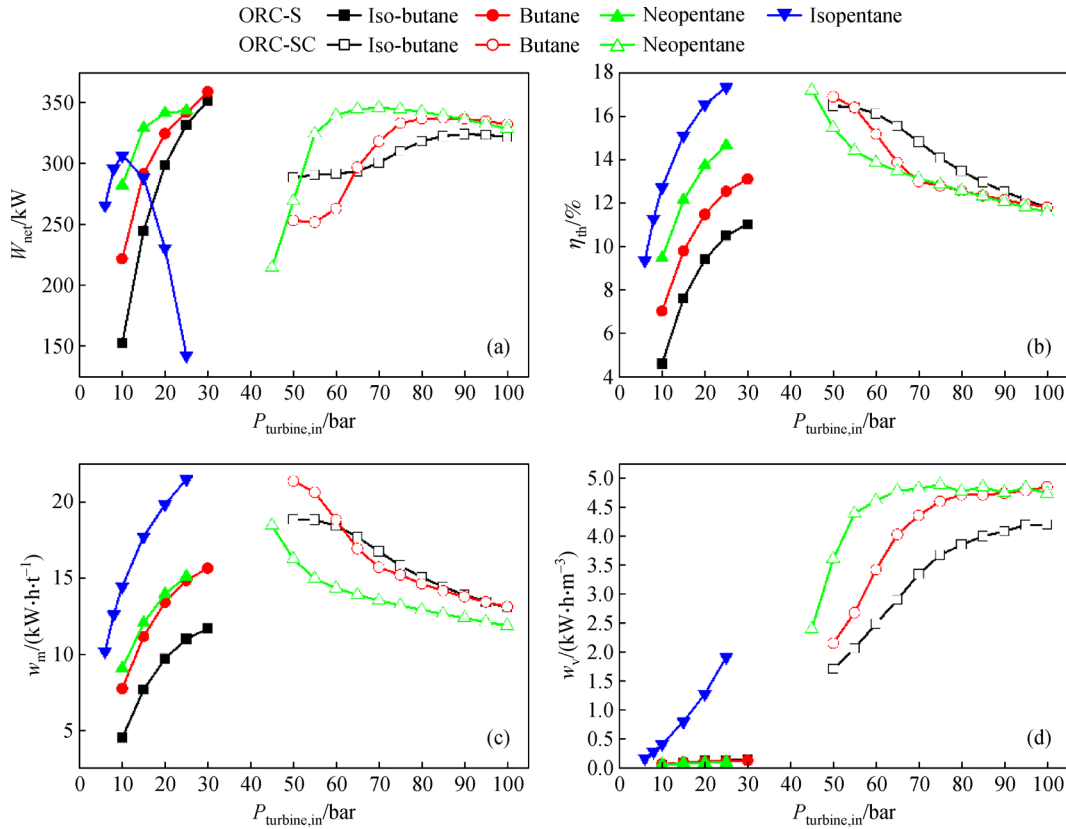


Fig. 8 Performance of ORCs with different dry fluids.
(a) W_{net} ; (b) η_{th} ; (c) w_m ; (d) w_v .

conclusion can be drawn that the ORC-SC is more suitable for wet fluids, but it is not recommended to apply a $P_{\text{turbine,in}}$ as high as the equipment can withstand. Overall, the selected wet fluids with the ORC-SC have the capability to generate maximum W_{net} values of around 330 kW, except for the fluid propyne of the highest T_c among the wet fluids.

Because the isopentane has a T_c exceeding the temperature that the superheater can support, it cannot arrive at the supercritical state in this paper. Therefore, it is only tested with the ORC-S. Except for the fluid isopentane, Fig. 8 describes the thermodynamic properties of the other selected dry fluids both with the ORC-S and ORC-SC. The fluid types are also arranged in ascending order of critical temperature at the top. The solid signs still stand for the values derived from the ORC-S, while the hollow signs represent the results obtained from the ORC-SC. Because of the abrupt change of the temperature at the inlet of the turbine from saturation to supercritical state, the curves of the ORC-S mode and the ORC-SC mode are discrete around the critical point. As Fig. 8 shows, increasing the $P_{\text{turbine,in}}$ always benefits the four indicators of the ORC-S, but goes against the improvement of the η_{th} and the w_v of the ORC-SC. Besides, the ORC-SC only makes a tiny improvement in W_{net} of the dry fluid, like the

neopentane in Fig. 8(a), whose T_c is close to but less than the heat supply temperature. Therefore, it is not necessary to make a dry fluid supercritical in the view of W_{net} . In addition, although outstanding advantage of η_{th} , w_m , and w_v over the ORC-S can be obtained by adopting the ORC-SC as shown in Fig. 9, the issues of high operation pressure and large expansion ratio also result in the complexity and extra investment of design and operation. In the Gonghe Basin, it is not recommended to apply a dry fluid, such as isopentane, whose T_c is higher than the heat supply, for the relatively low turning point of W_{net} in Fig. 8(a).

5.3 Comparison of KCS-11 and ORCs

Table 4 tabulates the specific performance of each selected working fluid with the suitable cycle that output the maximum W_{net} . The working fluids for the ORCs are arranged from top to bottom in the ascending order of T_c . SC and SH stand for the supercritical state and superheated state at the turbine inlet, respectively. γ represents the vapor quality at the turbine outlet, and T_{inj} denotes the temperature of the heat carrier injected back into the EGS, that is, the temperature of the heat carrier leaving the bottoming cycle.

The η_{th} and η_{ex} values in Table 4 are nearly the same.

Table 4 Maximum W_{net} of bottoming cycles with different working fluids

Fluids	EM	$\eta_{th}/\%$	$\eta_{ex}/\%$	$w_m/(kW \cdot h \cdot t^{-1})$	$w_v/(kW \cdot h \cdot m^{-3})$	W_{net}/kW	$P_{turbine,in}/bar$	$T_{inj}/^{\circ}C$	$\gamma/\%$
76% NH ₃	SH	14.03	48.30	40.00	0.62	246.01	30	111.45	0.95
78% NH ₃	SH	13.45	47.19	38.54	0.59	256.55	30	104.86	0.96
80% NH ₃	SH	13.61	48.76	41.81	0.75	279.99	35	98.47	0.95
82% NH ₃	SH	13.17	48.90	40.57	0.73	302.31	35	88.17	0.96
84% NH ₃	SH	12.74	47.69	39.59	0.71	298.90	35	86.03	0.96
86% NH ₃	SH	12.26	46.05	38.72	0.69	290.83	35	84.87	0.97
88% NH ₃	SH	11.73	44.20	37.72	0.67	281.36	35	83.74	0.98
Propylene	SC	12.62	49.08	14.08	2.13	329.63	85	74.49	SH
Propane	SC	12.67	49.22	14.29	2.46	330.58	85	74.65	SH
Cyclopropane	SC	12.65	49.44	15.28	3.72	334.21	95	73.20	0.96
Dimethylether	SC	13.07	50.57	16.58	3.32	337.51	80	75.81	SH
Propyne	SC	15.11	54.28	23.98	2.42	318.44	65	96.25	SH
Isobutane	S	11.03	47.81	11.67	0.15	351.93	30	49.51	SH
Butane	S	13.09	52.08	15.65	0.13	359.21	30	68.82	SH
Neopentane	SC	13.13	51.26	13.51	4.82	345.91	60	73.53	SH
Isopentane	S	12.70	47.80	14.43	0.41	306.86	10	82.98	SH

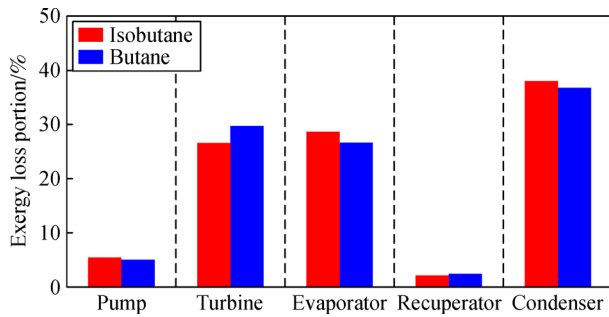


Fig. 9 Exergy destruction portion occupied by each device.

The KCS-11 occupies the superiority of w_m over the others, while the ORC-SC results in a higher w_v . The KCS-11 and ORC-S allow the whole system to operate under a fairly low pressure, reducing the equipment investment and the operation and maintenance costs. Besides, because the heat carrier leaving the bottoming cycle is commonly injected back in the EGS directly, a higher T_{inj} actually indicates a failure to take maximum use of the extracted heat. It should be emphasized that the W_{net} directly determined the profits of the prospective HDR power plant in the long run. Therefore, the combination and results in Table 4 are compared in terms of the W_{net} indicator.

According to Fig. 6 and Table 4, an AMF of 82% enables the KCS-11 to generate the highest W_{net} of 302.31 kW of all the AMFs proposed in the Gonghe Basin scenario. Even though it is well known that the KCS-11 has the superiority over the KCS-34 and KCS-34 g when dealing with a heat source of about 121°C to 204°C, the best performance in W_{net} of the KCS-11 still cannot match

that of the ORCs.

Figures 7 and 8 prove the advantages of the ORC-SC and ORC-S respectively for wet and dry fluids. The highest W_{net} (337.51 kW) of wet fluids is yielded by the combination of the ORC-SC and the fluid dimethylether. The dry fluids perform a better W_{net} than the above KCS-11 and the ORC combined with wet fluids. Generating a W_{net} output as high as 359.21 kW, the ORC-S with the dry fluid butane is suggested as the most suitable choice for the Gonghe Basin. The dry fluid isobutane can also be reserved as an alternative option.

To further realize the cycle characteristics, the exergy destruction and exergy efficiency of each device in the ORC-Ss combined with isobutane and butane are analyzed and illustrated in Figs. 9 and 10, respectively. As shown in Fig. 9, the turbine, the evaporator, and the condenser are the main devices that suffer from exergy destruction. The reason for the difference between the exergy destructions of the turbines is that, the output of the butane turbine is

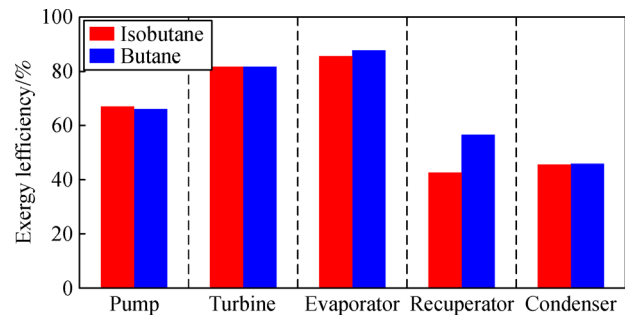


Fig. 10 Exergy efficiency of each device.

relatively higher than that of the isobutane turbine. Except for the recuperators, the other corresponding device pairs perform nearly the same exergy efficiency as each other, as shown in Fig. 10. The fluid butane enables its recuperator to provide a higher exergy efficiency, which means the butane has a better capability for heat recovery.

6 Conclusions

A prospective study was conducted to investigate the exploitation and utilization of the detected HDR resources in the Gonghe Basin, Qinghai province. Based on a comparison with certain proven HDR resources worldwide, it is predicted that it could provide high-temperature hot water of 185°C at a flowrate of 20 t/h. Under these heat production conditions, seven KCS-11 cases with different AMFs and three ORC configurations selectively combined with 9 pure working fluids were compared, from which it is concluded that:

For the bottoming KCS-11, an AMF of 82% can generate the most net power output, which is 302.3 kW.

Dry fluids are more suitable for ORC-S, while wet fluids are more suitable for ORC-SC in terms of the net power output they yield.

Under the given heat production conditions of HDRs in the Gonghe Basin, the net power output of the ORC-S and dry fluids combinations is higher than that of the other ORCs, and is far higher than the output in all KCS-11 cases.

The ORC-S with butane as working fluid is most competitive of all bottoming cycle cases tested. Specifically, the maximum net power generated by this proposed combination is 359.2 kW.

Acknowledgements This work was supported by the State Grid Technology Program (SGRI-DL-71-15-006), and the Scientific and Technological Project of Qinghai Province, China (2018-ZJ-726).

Notations

AMF	Ammonia mass fraction
EGS	Enhanced geothermal system
HDR	Hot dry rock
K	State point in Kalina cycle
KC	Kalina cycle
KCS	Kalina cycle system
KCS-11	Kalina cycle system 11
KCS-34	Kalina cycle system 34
KCS-34 g	Kalina cycle system 34 g
O	State point in organic Rankine cycle
ORC	Organic Rankine cycle
ORC-S	Organic Rankine cycle with saturated expansion

ORC-SC	Organic Rankine cycle with supercritical expansion
ORC-SH	Organic Rankine cycle with superheated expansion
SC	Supercritical state
SH	Superheated state
D	Depth/m
P	Pressure/bar
T	Temperature/°C
W	Power output/MW
e	Specific exergy/(kJ·kg ⁻¹)
h	Specific enthalpy/(kJ·kg ⁻¹)
m	Mass flowrate/(t·h ⁻¹)
s	Specific entropy/(kJ·kg ⁻¹ ·°C ⁻¹)
v	Volume flowrate/(m ³ ·h ⁻¹)
w_m	Mass specific power/(kW·h·t ⁻¹)
w_v	Volume specific power/(kW·h·m ⁻³)
γ	Vapor quality/%
η	Efficiency/%
0	In ambient condition
c	At critical point
cold	At the cold side
ex	Parameter based on exergy
hot	At the hot side
i	At certain state point i
in	At the inlet
inj	At the inlet of injection well of EGS
net	Net power output
out	At the outlet
pro	At the outlet of production well of EGS
th	Parameter based on thermal energy

References

1. Mortensen J J. Hot dry rock: a new geothermal energy source. *Energy*, 1978, 3(5): 639–644
2. Lu S M. A global review of enhanced geothermal system (EGS). *Renewable & Sustainable Energy Reviews*, 2018, 81: 2902–2921
3. Breede K, Dzebisashvili K, Liu X, Falcone G. A systematic review of enhanced (or engineered) geothermal systems: past, present and future. *Geothermal Energy*, 2013, 1(1): 4
4. Tester J W, Anderson B J, Batchelor A S, Blackwell D D, DiPippo R, Drake E M, Garnish J, Livesay B, Moore M C, Nichols K, Petty S, Toksoz M N, Veatch R W, Baria R, Augustine C, Murphy E, Negraru P, Richards M. Impact of enhanced geothermal systems on US energy supply in the twenty-first century. *Philosophical Transactions of the Royal Society A: Mathematical, Physical and Engineering Sciences*, 1853, 2007(365): 1057–1094
5. Cao W, Huang W, Wei G, Jin Y, Jiang F. A numerical study of non-Darcy flow in EGS heat reservoirs during heat extraction. *Frontiers in Energy*, 2019, 13(3): 439–449

6. Guo J, Cao W, Wang Y, Jiang F. A novel flow-resistor network model for characterizing enhanced geothermal system heat reservoir. *Frontiers in Energy*, 2019, 13(1): 99–106
7. Larjola J. Electricity from industrial waste heat using high-speed organic Rankine cycle (ORC). *International Journal of Production Economics*, 1995, 41(1–3): 227–235
8. Hung T C, Shai T Y, Wang S K. A review of organic Rankine cycles (ORCs) for the recovery of low-grade waste heat. *Energy*, 1997, 22 (7): 661–667
9. Liu B, Chien K, Wang C. Effect of working fluids on organic Rankine cycle for waste heat recovery. *Energy*, 2004, 29(8): 1207–1217
10. Mago P J, Chamra L M, Srinivasan K, Somayaji C. An examination of regenerative organic Rankine cycles using dry fluids. *Applied Thermal Engineering*, 2008, 28(8–9): 998–1007
11. Tomarov G V, Shipkov A A. Modern geothermal power: binary cycle geothermal power plants. *Thermal Engineering*, 2017, 64(4): 243–250
12. Quick H, Michael J, Huber H, Arslan U. History of international geothermal power plants and geothermal projects in Germany. In: *Proceedings of World Geothermal Congress 2010, Bali, Indonesia, 2010*
13. Campos Rodríguez C E, Escobar Palacio J C, Venturini O J, Silva Lora E E, Cobas V M, Marques dos Santos D, Lofrano Dotto F R, Gialluca V. Exergetic and economic comparison of ORC and Kalina cycle for low temperature enhanced geothermal system in Brazil. *Applied Thermal Engineering*, 2013, 52(1): 109–119
14. Kalina A I. Combined cycle and waste heat recovery power systems based on a novel thermodynamic energy cycle utilizing low-temperature heat for power generation. In: *1983 Joint Power Generation Conference, Indianapolis, Indiana, USA, 1983*
15. Thorin E, Dejfors C, Svedberg G. Thermodynamic properties of ammonia–water mixtures for power cycles. *International Journal of Thermophysics*, 1998, 19(2): 501–510
16. Prananto L A, Zaini I N, Mahendranata B I, Juangsa F B, Aziz M, Soelaiman T A F. Use of the Kalina cycle as a bottoming cycle in a geothermal power plant: case study of the Wayang Windu geothermal power plant. *Applied Thermal Engineering*, 2018, 132: 686–696
17. Singh O K, Kaushik S C. Energy and exergy analysis and optimization of Kalina cycle coupled with a coal fired steam power plant. *Applied Thermal Engineering*, 2013, 51(1–2): 787–800
18. He J, Liu C, Xu X, Li Y, Wu S, Xu J. Performance research on modified KCS (Kalina cycle system) 11 without throttle valve. *Energy*, 2014, 64: 389–397
19. Mlcak H A. Kalina cycle® concepts for low temperature geothermal. *Transactions–Geothermal Resources Council*, 2002, 26(26): 707–713
20. Zhang X, He M, Zhang Y. A review of research on the Kalina cycle. *Renewable & Sustainable Energy Reviews*, 2012, 16(7): 5309–5318
21. Leibowitz H, Mirolli M. First Kalina combined-cycle plant tested successfully. *Power Engineering*, 1997, 10(55): 44
22. Mlcak H, Mirolli M, Hjartarson H, Húsavíkur O. Notes from the north: a report on the debut year of the 2 MW Kalina cycle® geothermal power plant in Húsavík, Iceland. *Transactions–Geothermal Resources Council*, 2002, 26: 715–718
23. Victor R A, Kim J K, Smith R. Composition optimisation of working fluids for organic Rankine cycles and Kalina cycles. *Energy*, 2013, 55: 114–126
24. Chen H. The conversion of low-grade heat into power using supercritical Rankine cycles. *Dissertation for the Doctoral Degree*. Florida: University of South Florida, 2010
25. Saleh B, Koglbauer G, Wendland M, Fischer J. Working fluids for low-temperature organic Rankine cycles. *Energy*, 2007, 32(7): 1210–1221
26. Dai Y, Wang J, Gao L. Parametric optimization and comparative study of organic Rankine cycle (ORC) for low grade waste heat recovery. *Energy Conversion and Management*, 2009, 50(3): 576–582
27. Geox GmbH. *Geothermal electricity generation in Landau. 2020–02–12*, available at website of BINE Information Service–Publications
28. Mergner H, Weimer T. Performance of ammonia-water based cycles for power generation from low enthalpy heat sources. *Energy*, 2015, 88: 93–100
29. Lin D, Zhu Q, Li X. Thermodynamic comparative analyses between (organic) Rankine cycle and Kalina cycle. *Energy Procedia*, 2015, 75: 1618–1623
30. Fiaschi D, Manfrida G, Rogai E, Talluri L. Exergoeconomic analysis and comparison between ORC and Kalina cycles to exploit low and medium-high temperature heat from two different geothermal sites. *Energy Conversion and Management*, 2017, 154: 503–516
31. Gholamian E, Zare V. A comparative thermodynamic investigation with environmental analysis of waste heat to power conversion employing Kalina and organic Rankine cycles. *Energy Conversion and Management*, 2016, 117: 150–161
32. Eller T, Heberle F, Brüggemann D. Second law analysis of novel working fluid pairs for waste heat recovery by the Kalina cycle. *Energy*, 2017, 119: 188–198
33. Bombarda P, Invernizzi C M, Pietra C. Heat recovery from Diesel engines: a thermodynamic comparison between Kalina and ORC cycles. *Applied Thermal Engineering*, 2010, 30(2–3): 212–219
34. Elsayed A, Embaye M, AL-Dadah R, Mahmoud S, Rezk A. Thermodynamic performance of Kalina cycle system 11 (KCS11): feasibility of using alternative zeotropic mixtures. *International Journal of Low Carbon Technologies*, 2013, 8(suppl 1): i69–i78
35. Yue C, Han D, Pu W, He W. Comparative analysis of a bottoming transcritical ORC and a Kalina cycle for engine exhaust heat recovery. *Energy Conversion and Management*, 2015, 89: 764–774
36. Nemati A, Nami H, Ranjbar F, Yari M. A comparative thermodynamic analysis of ORC and Kalina cycles for waste heat recovery: a case study for CGAM cogeneration system. *Case Studies in Thermal Engineering*, 2017, 9: 1–13
37. Yari M, Mehr A S, Zare V, Mahmoudi S M S, Rosen M A. Exergoeconomic comparison of TRC (trilateral Rankine cycle), ORC (organic Rankine cycle) and Kalina cycle using a low grade heat source. *Energy*, 2015, 83: 712–722
38. U.S. Department of Energy. *Environmental assessment and finding of no significant impact: Kalina geothermal demonstration project steamboat springs, Nevada*. Office of Scientific & Technical Information Technical Reports, 1999

39. Prananto L A, Soelaiman T M F, Aziz M. Adoption of Kalina cycle as a bottoming cycle in Wayang Windu geothermal power plant. *Energy Procedia*, 2017, 142: 1147–1152
40. Zhang X, Yang S, Yang Z. *The Plate Tectonics of Qinghai Province—A Guide to the Geotectonic Map of Qinghai Province*. Beijing: Geological Publishing House, 2007 (in Chinese)
41. Zhang S, Yan W, Li D, Jia X, Zhang S, Li S, Fu L, Wu H, Zeng Z, Li Z, Mu J, Cheng Z, Hu L. Characteristics of geothermal geology of the Qiabuqia HDR in Gonghe Basin, Qinghai Province. *Geology in China*, 2018, 45(6): 1087–1102 (in Chinese)
42. Bruel D. Heat extraction modelling from forced fluid flow through stimulated fractured rock masses: application to the Rosemanowes hot dry rock reservoir. *Geothermics*, 1995, 24(3): 361–374
43. Tenma N, Iwakiri S I, Matsunaga I. Development of hot dry rock technology at Hijiori test site: program for a long-term circulation test. *Energy Sources*, 1998, 20(8): 753–762
44. Hori Y, Kitano K, Kaieda H, Kiho K. Present status of the Ogachi HDR project, Japan, and future plans. *Geothermics*, 1999, 28(4–5): 637–645
45. Duchane D V. Geothermal energy production from hot dry rock: operational testing at the Fenton Hill, New Mexico HDR test facility. In: *Energy-sources Technology Conference and Exhibition*, New Orleans, LA, USA, 1994
46. GeothermEx Inc. Data review of the hot dry rock project at Fenton Hill, New Mexico. Office of Scientific & Technical Information Technical Reports, 1998
47. Duchane D, Brown D. Hot dry Rock (HDR) geothermal energy research and development at Fenton Hill, New Mexico. *GHC Bulletin*, 2002, 9: 13–19
48. Brown D W. Hot dry rock geothermal energy: important lessons from Fenton Hill. In: *Proceedings of 34th Workshop on Geothermal Reservoir Engineering*, 2009
49. Kelkar S, WoldeGabriel G, Rehfeldt K. Lessons learned from the pioneering hot dry rock project at Fenton Hill, USA. *Geothermics*, 2016, 63: 5–14
50. Guo C, Pan L, Zhang K, Oldenburg C M, Li C, Li Y. Comparison of compressed air energy storage process in aquifers and caverns based on the Huntorf CAES plant. *Applied Energy*, 2016, 181: 342–356
51. Zhang T, Chen L, Zhang X, Mei S, Xue X, Zhou Y. Thermodynamic analysis of a novel hybrid liquid air energy storage system based on the utilization of LNG cold energy. *Energy*, 2018, 155: 641–650
52. Bassily A M. Modeling, numerical optimization, and irreversibility reduction of a triple-pressure reheat combined cycle. *Energy*, 2007, 32(5): 778–794
53. Zhang T, Zhang X L, He Y L, Xue X D, Mei S W. Thermodynamic analysis of hybrid liquid air energy storage systems based on cascaded storage and effective utilization of compression heat. *Applied Thermal Engineering*, 2020, 164: 114526
54. Uusitalo A, Honkatukia J, Turunen-Saaresti T. Evaluation of a small-scale waste heat recovery organic Rankine cycle. *Applied Energy*, 2017, 192: 146–158